

Seminar paper

Cognitive and brain science

Iron, Lipid & R1 correlation

**written by Shirly Eliezer,
Mezer lab, ELSC**

Table of contents

Title page	1
Table of contents	2
Abstract	<u>3</u>
Introduction	<u>3</u> -4
Methods	<u>4</u> -8
Results	<u>8</u> -10
Discussion	<u>11</u>
References	<u>12</u>

Abstract

Quantitative magnetic resonance imaging (qMRI) provides biophysical parametric measurements allowing for noninvasive mapping of the aging human brain. One of the qMRI parameter is T1, longitudinal relaxation time, the time constant which determines the rate at which excited protons return to equilibrium. The literature indicates that lipids have strongly affect the contrast of brain qMRI maps. The iron content and water fraction (WF) of cellular compartments are also known as influence the qMRI parameters. There have been a few quantitative attempts to find a relationship between lipid content and T1. Additionally, it is unclear how much iron content contributes to T1 tissue contrast. In this research, we aim to find the best describes the relationship between iron and lipid to R1.

Introduction

Advances in the field of magnetic resonance imaging (MRI) have led to the development of quantitative MRI (qMRI). qMRI provides biophysical parametric measurements that are useful in the investigation and diagnosis of normal and abnormal aging (Callaghan, et al., 2014; Yeatman, Wandell & Mezer, 2016; Gracien et al., 2017).

qMRI is aimed at the direct measurement of the physical tissue properties. Tissue can be characterized by two different relaxation times - T1 and T2. T1 (longitudinal relaxation time) is the time constant which determines the rate at which excited protons return to equilibrium. In this study we will focus on the longitudinal relaxation rate ($R1=1/T1$). It is a measure of the time taken for spinning protons to realign with the external magnetic field. (Neurology, 2016).

qMRI enables the creation of parametric maps which allows a reliable comparison of brain structure across different time points and different MRI scanners, making it possible to assess normal brain development, as well as pathological conditions.

The human brain is comprised mainly of water (70–80%), proteins (8–11%) and lipids (5–15%) (add ref). The distribution of these molecules varies between brain regions, across lifespan, and in different pathological states. Lipids are known to strongly affect the contrast of brain qMRI maps. (Shtangel & Mezer, 2020)

Iron is an important metal involved in various physiological processes, such as ATP generation and DNA replication (Chang, 2019; Mills et al., 2010; Qian & Ke, 2019).

Particularly, iron is essential for a variety of neurological processes (McCarthy & Kosman, 2015; Rouault, 2013). Iron transport in the brain is effectuated by several pathways; namely, transferrin-dependent iron transport, non-transferrin bound iron (NTBI) mobilization, uptake and export by and from neurons, oligodendrocytes, astrocytes, and microglia (Hohnholt & Dringen, 2013; Roy Sarkar & Dutta, 2019). Furthermore, Ferritin is the main iron storage protein, conformed by two types of subunits, H type (heavy) and L type (light), which co-assemble into a supramolecular spherical-shaped protein (Chang, 2019). The iron content and water fraction (WF) of cellular compartments are thought to influence the qMRI parameters (Shtangel & Mezer, 2020).

There have been a few quantitative attempts to find a relationship between lipid content and T1 (Bot et al., 2004; Mottershead et al., 2003; Schmierer et al., 2004). Due to restricts in conventional imaging techniques in directly measuring the lipids concentration, the relationship between T1 and lipids remain vague. Additionally, it is unclear how much iron content contributes to T1 tissue contrast (Gelman et al., 2001). The literature regarding iron and T1 contrast is controversial: data showing a clear relationship between brain T1 and iron concentration (Ogg and Steen, 1998; Vymazal et al., 1995) contradict other publications showing no significant correlation of T1 and iron (Steen et al., 2000).

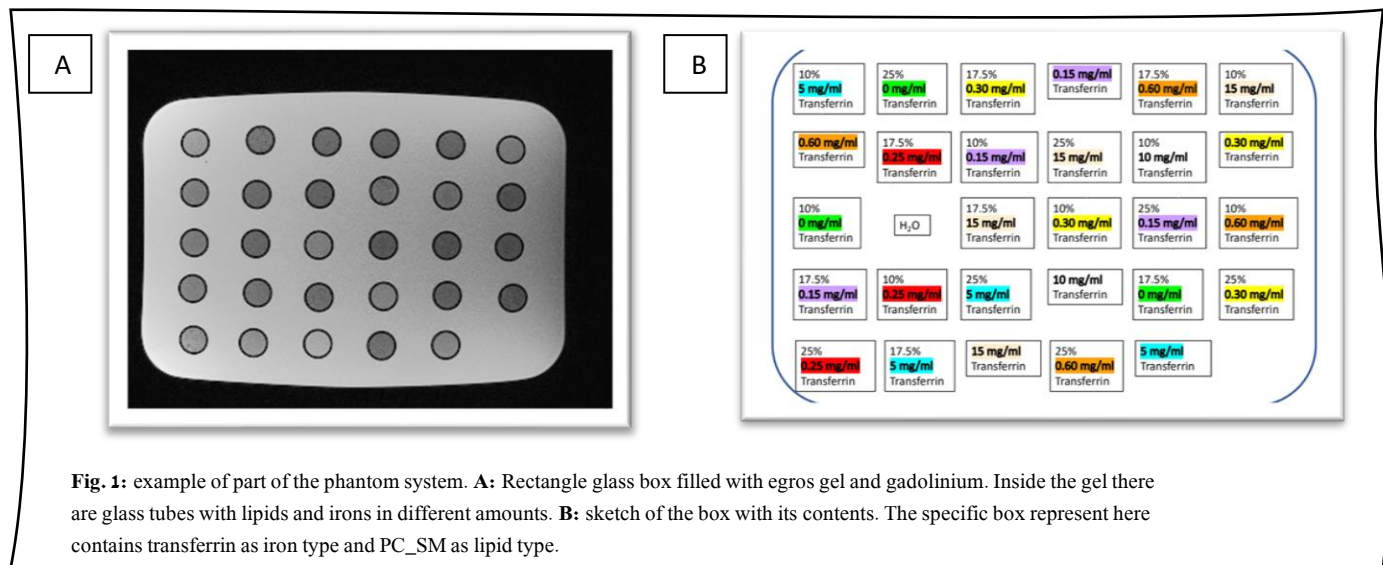
The main objective of this work was to deduce a model representing the effect of lipids and iron on qMRI parameters, specifically R1 ($1/T1$).

Methods

Data collection

This study describes a phantom system designed to assess the contribution of various membrane lipids and irons to qMRI parameters using a clinical human scanner. Three lipid types have been chosen: phosphatidylcholine (PC), phosphatidylcholine sphingomyelin (PC_SM), and phosphatidylcholine cholesterol (PC_Chol). In addition, 3 iron types have been chosen for the experiment: Fe²⁺, Ferritin, Transferrin.

The phantom systems composed of several boxes; each contains approximately 29 test tubes. Common to each box in the lipid type and iron type. Each test tube in each box contains different concentration of lipid and different concentration of iron, as seen in fig. 1.



Each box scanned in 3 T MRI machine, and qMRI parameters were established. The entire data of the phantom system is represented in a csv file as seen in fig. 2, contains all the samples information, and the qMRI parameters as received from qMRI analyses.

	A	B	C	D	E	F	G	H	I	J	K	L	M	N	O	P	Q	R	S	T	U	V	W	X	Y	Z	AA	AB	AC	AD	AE	AF	AG	AH	AI	AJ	AK	AL	AM	AN	AO	AP	AQ	AR	AS	AT	AU	AV	AW	AX	AY	AZ	BA	BB	BC	BD	BE	BF	BG	BH	BI	BJ	BK	BL	BM	BN	BO	BP	BQ	BR	BS	BT	BU	BV	BW	BX	BY	BZ	CA	CB	CC	CD	CE	CF	CG	CH	CI	CJ	CK	CL	CM	CN	CO	CP	CQ	CR	CS	CT	CU	CV	CW	CX	CY	CZ	DA	DB	DC	DD	DE	DF	DG	DH	DI	DJ	DK	DL	DM	DN	DO	DP	DQ	DR	DS	DT	DU	DV	DW	DX	DY	DZ	EA	EB	EC	ED	EE	EF	EG	EH	EI	EJ	EK	EL	EM	EN	EO	EP	EQ	ER	ES	ET	EU	EV	EW	EX	EY	EZ	FA	FB	FC	FD	FE	FF	FG	FH	FI	FJ	FK	FL	FM	FN	FO	FP	FQ	FR	FS	FT	FU	FV	FW	FX	FY	FZ	GA	GB	GC	GD	GE	GF	GG	GH	GI	GJ	GK	GL	GM	GN	GO	GP	GQ	GR	GS	GT	GU	GV	GW	GX	GY	GZ	HA	HB	HC	HD	HE	HF	HG	HH	HI	HJ	HK	HL	HM	HN	HO	HP	HQ	HR	HS	HT	HU	HV	HW	HX	HY	HZ	IA	IB	IC	ID	IE	IF	IG	IH	II	IJ	IK	IL	IM	IN	IO	IP	IQ	IR	IS	IT	IU	IV	IW	IX	IY	IZ	JA	JB	JC	JD	JE	JF	JG	JH	JI	IJ	JK	JL	JM	JN	JO	JP	JQ	JR	JS	JT	JU	JV	JW	JX	JY	JZ	KA	KB	KC	KD	KE	KF	KG	KH	KI	KJ	KK	KL	KM	KN	KO	KP	KQ	KR	KS	KT	KU	KV	KW	KX	KY	KZ	LA	LB	LC	LD	LE	LF	LG	LH	LI	LJ	LK	LM	LN	LO	LP	LQ	LR	LS	LT	LU	LV	LW	LX	LY	LZ	MA	MB	MC	MD	ME	MF	MG	MH	MI	MJ	MK	ML	MM	MN	MO	MP	MQ	MR	MS	MT	MU	MV	MW	MX	MY	MZ	NA	NB	NC	ND	NE	NF	NG	NH	NI	NJ	NK	NL	NM	NN	NO	NP	NQ	NR	NS	NT	NU	NV	NW	NX	NY	NZ	OA	OB	OC	OD	OE	OF	OG	OH	OI	OJ	OK	OL	OM	ON	OO	OP	OQ	OR	OS	OT	OU	OV	OW	OX	OY	OZ	PA	PB	PC	PD	PE	PF	PG	PH	PI	PJ	PK	PL	PM	PN	PO	PP	PQ	PR	PS	PT	PU	PV	PW	PX	PY	PZ	QA	QB	QC	QD	QE	QF	QG	QH	QI	QJ	QK	QL	QM	QN	QO	QP	QQ	QR	QS	QT	QU	QV	QW	QX	QY	QZ	RA	RB	RC	RD	RE	RF	RG	RH	RI	RJ	RK	RL	RM	RN	RO	RP	RQ	RR	RS	RT	RU	RV	RW	RX	RY	RZ	SA	SB	SC	SD	SE	SF	SG	SH	SI	SJ	SK	SL	SM	SN	SO	SP	SQ	SR	SS	ST	SU	SV	SW	SX	SY	SZ	TA	TB	TC	TD	TE	TF	TG	TH	TI	TJ	TK	TL	TM	TN	TO	TP	TQ	TR	TS	TT	TU	TV	TW	TX	TY	TZ	UA	UB	UC	UD	UE	UF	UG	UH	UI	UJ	UK	UL	UM	UN	UO	UP	UQ	UR	US	UT	UU	UV	UW	UX	UY	UZ	VA	VB	VC	VD	VE	VF	VG	VH	VI	VJ	VK	VL	VM	VN	VO	VP	VQ	VR	VS	VT	VU	VV	VW	VX	VY	VZ	WA	WB	WC	WD	WE	WF	WG	WH	WI	WJ	WK	WL	WM	WN	WO	WP	WQ	WR	WS	WT	WU	WV	WW	WX	WY	WZ	XA	XB	XC	XD	XE	XF	XG	XH	XI	XJ	XK	XL	XM	XN	XO	XP	XQ	XR	XS	XT	XU	XV	XW	XX	XY	XZ	YA	YB	YC	YD	YE	YF	YG	YH	YI	YJ	YK	YL	YM	YN	YO	YP	YQ	YR	YS	YT	YU	YV	YW	YX	YZ	ZA	ZB	ZC	ZD	ZE	ZF	ZG	ZH	ZI	ZJ	ZK	ZL	ZM	ZN	ZO	ZA	ZB	ZC	ZD	ZE	ZF	ZG	ZH	ZI	ZJ	ZK	ZL	ZM	ZN	ZO
1	Protein	(mg/ml)	iron (mg/ml)	lipid (%)	MTV exp	R1 [1/sec]	F2 [1/sec]	MTV fraction	R2 [1/sec]	I1 type	estimation	(mg/iron type	lipid type	expNurFe	sigma (mg/ml)																																																																																																																																																																																																																																																																																																																																																																																																																																																																																																																																																																																																																																																																																																																	

Pre-processing of the data

Out of 10 experiments (273 samples), 2 were disqualified. 1 experiment was disqualified due to inaccurate amounts of substances and the other was disqualified due to the fact it contains protein that was irrelevant for the current research.

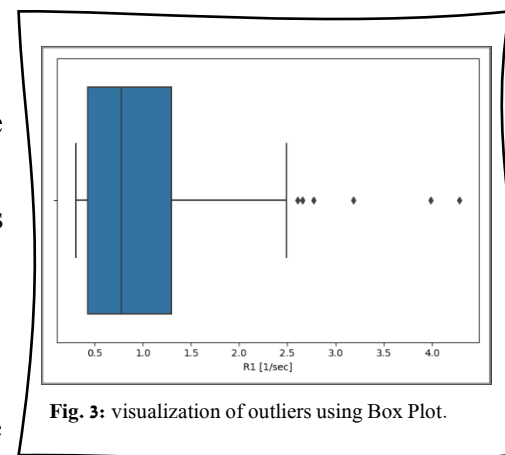
Outliers

To detect outliers, calculation of Z-score was made. Z-score is a statistical measure represent the number of standard deviations away from the mean that a certain data point is. The equation of Z-score calculated as follows: $Z = \frac{x-\mu}{\sigma}$ where μ =mean of the R1 values X; σ =Standard deviation of the R1; X= R1. Z-score values greater than or less than + 3 or - 3, respectively, are considered outliers (Misra et al., 2019; Tabachnick & Fidell, 2013).

Visualization of the outliers was created by using box plot. A boxplot is another convenient approach to identifying univariate outliers (Field & Miles, 2010; Tukey, 1977) which graphically depicting groups of numerical data through their quartiles. It has lines extending vertically from the boxes (whiskers) indicating variability outside the upper and lower quartiles. As seen in fig. 3, outliers can be detected outside the upper quartiles.

After calculating Z-score for the R1 values, values with distance of 3 SD and more from the mean, were disqualified (3 samples).

After performing pre-processing methods on the data, 163 samples remain.



Relationship between the variables.

To assess the relationship between the independent variables and the dependent variable, Pearson's correlation coefficient was calculated. The correlation coefficient is a measure of linear correlation between two sets of data (Correlation Coefficient, 2021; Pearson, 1895). The Pearson correlation coefficient calculated by dividing the covariance of the two variables, with the products of their standard deviations. $P =$

$$\frac{COV(X,Y)}{\sigma_X \cdot \sigma_Y}. \text{ The covariance is calculated as follows: } COV(X,Y) = \frac{E[(X-\mu_X)(Y-\mu_Y)]}{\sigma_X \cdot \sigma_Y}.$$

Linear Regression Models

Simple linear regression models were created to examine the ability to predict R1 values by iron and lipid concentrations. Linear regression is a linear approach for modelling the relationship between a scalar response and one or more explanatory variables (Freedman, 2009).

In this research, the response is the R1 (1/sec) values, which derived from T1 results ($R1 = 1/T1$), and the explanatory variables are the lipid and iron concentrations.

As mentioned earlier, the research focuses on 3 different iron types: Fe2, Ferritin and Transferrin. In order to address the iron concentration, bound to the proteins (Ferritin, Transferrin), calculation of estimated Fe concentration.

In the first stage, simple and multiple linear regression were calculated. The equations were:

1. $R1 = a*[Fe] + b$
2. $R1 = a*[lipid] + b$
3. $R1 = a*[Fe] + b*[lipid] + c$

In the second stage, multiple linear regression with interaction model was created, based on the calculation $R1 = a*[Fe] + b*[lipid] + c*[Fe]*[lipid] + d$.

The third stage included linear regression with categorical variables; iron types and lipid types, to understand how the different types affects the relation between the substance's concentration and the target. The calculation of the model was as follows: $R1 = a*[lipid]*lipid\ type + b * [Fe] * iron\ type + c$. To properly use the categorical variables, encoded with dummy variables was established. In this stage, column of every iron type and lipid type added to the data frame. The code '1' presented in the column represented the iron type used in each sample, as well as lipid type (Fig. 4).

Lipid type_PC_SM	Lipid type_PC_Cholest	Lipid type_PC	Iron type_Transferrin	Iron type_Ferritin	Iron type_Fe2	[%] lipid	sigma [mg/ml] [Fe]	
0	1	0	0	0	1	10.0	0.000000	0
0	1	0	0	0	1	17.5	0.150000	1
0	1	0	0	0	1	25.0	0.600000	2
0	1	0	0	0	1	17.5	0.300000	4

Fig. 4: Dummy variables coding. 3 columns of iron types exchange the original column of the iron type, and so for the lipid type. The number 1 was written in the right column fit to the types used in the sample. In this example we can detect 4 samples with iron type Fe2 and lipid type PC_Cholest.

For the convenience, there will be use in this research in the equation $R1 = a*[lipid]*lipid\ type + b*[Fe]*iron\ type + c$ when in fact in the current technique, each iron type and each lipid type demonstrated different coefficient. In this way, when the sample involved Fe2 as iron type and PC as lipid type, the regression equation was: $R1 = a*[Fe]*Fe2(==1) + b*[lipid]*PC + c$. whereas for different iron type **a** coefficient will be different, same as the **b** coefficient.

To evaluate the goodness of fit of a model, R^2 coefficient of determination was calculated (Renaud et al., 2010). R^2 is a statistical measure of how well the regression predictions approximate the real data points. An R^2 of 1 indicates that the regression

predictions perfectly fit the data. $R^2 = \frac{TSS - RSS}{TSS}$ where RSS is the sum of squares of residuals, a measure of the discrepancy between the data and an estimation model and TSS is the total sum of squares - sum over all squared differences between the observations and their overall mean.

Furthermore, the mean absolute error was calculated. The mean absolute error is a way of comparing forecasts with their eventual outcomes (Willmott et al., 2005). The

calculation is as follows $MAE = \frac{\sum_{k=1}^n |y_i - \hat{y}|}{n}$ where n is the total number of the samples, y_i is specific value from the measured samples and \hat{y} is the predicted value.

Cross validation

Cross-validation is a data resampling method to assess the generalization ability of predictive models and to prevent overfitting (Hastie et al., 2008; Duda et al., 2001).

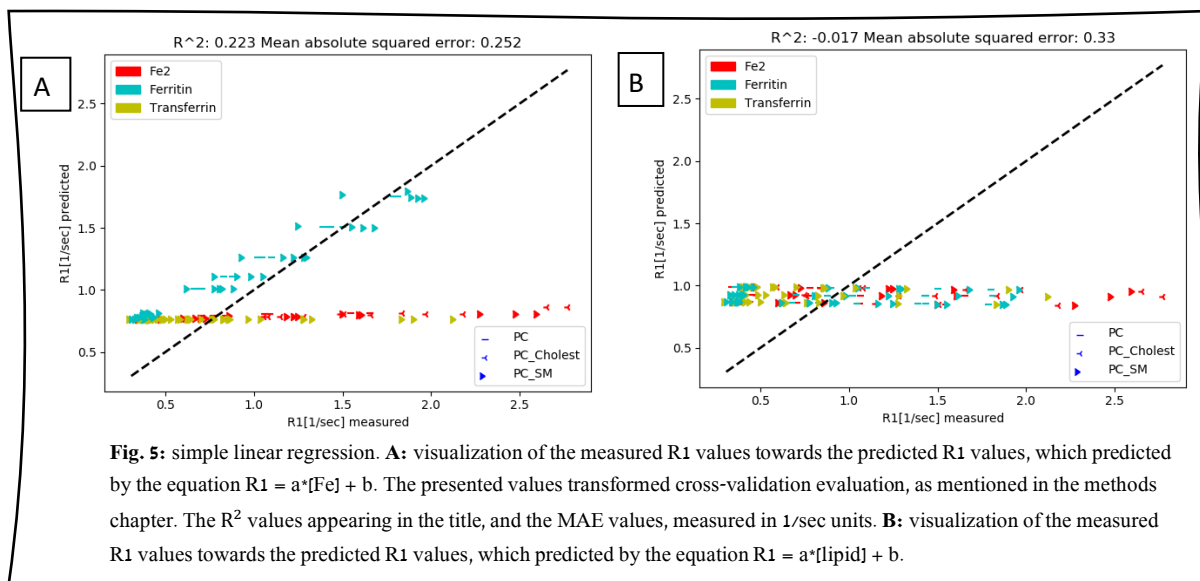
A central question in supervised learning concerns the accuracy of the resulting model. Overfitting is the case where a model is perfectly adapted to the data set at hand but then unable to generalize well to new, unseen data (Berrar et al., 2013). In this research, leave one out cross-validation technique was obtained. the available learning set is partitioned into n disjoint. The model is trained using n – 1 subsets, which, together, represent the training set. Then, the model is applied to the remaining subset, which is denoted as the validation set, and the performance is measured. This procedure is repeated until each of the n subsets has served as validation set. The average of the n performance measurements on the n validation sets is the cross-validated performance. The test error in LOOCV is approximately an unbiased estimate of the true prediction error (Hastie et al., 2008).

Results

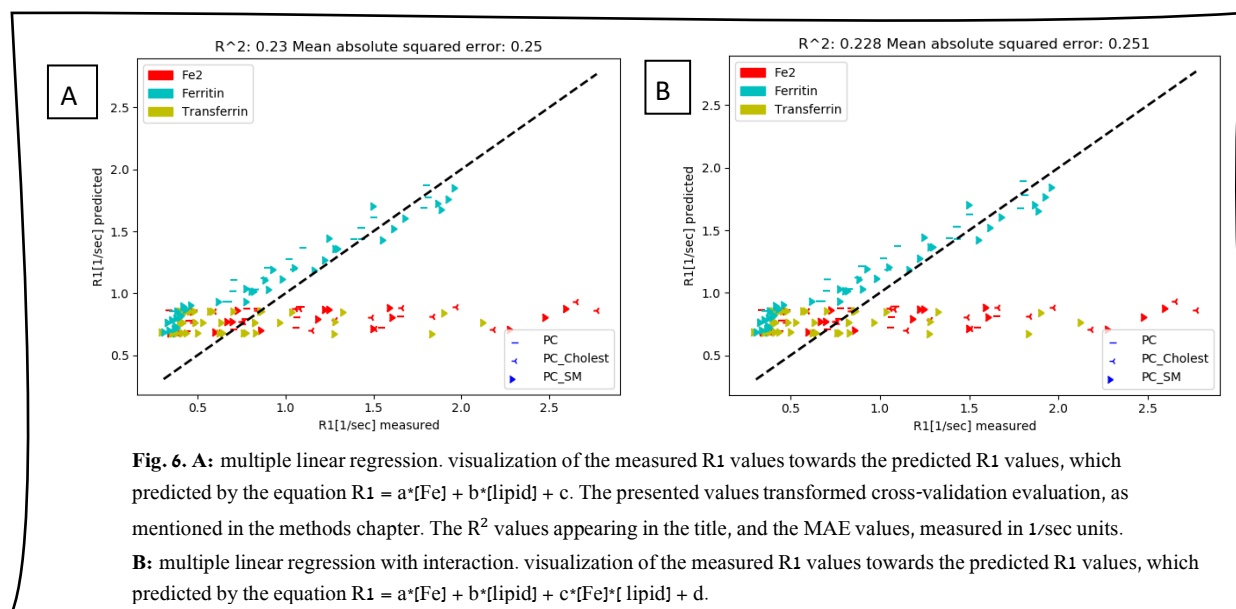
Pearson correlation coefficients was calculated for R1 target variable. It can be determined that p value smaller than 0.5 doesn't indicated strong linear relation (Mukaka, 2012; Benesty et al., 2009). The results indicated no significant relationship between R1 and iron concentrations ($p = 0.485$, $N=163$), and R1 to lipid concentrations ($p=0.086$, $N=163$).

Accordingly, simple Linear regression model created; $R1 = a[Fe] + b$, $R1 = a[lipid] + b$. Both models yielded low R^2 values, indicating a model that does not properly

explain the dependent variable by the independent variable (Hamilton, Ghert & Simpson, 2015), as seen in fig. 5.



Multiple linear regression and multiple linear regression with interaction were performed to evaluate the abilities of iron concentrations and lipids to predict R1 values as can be seen in Fig. 6.



It can be identified in fig.6 that groups of samples with the same iron type, and the same lipid type, have common slope, and the clustering of the iron types is more noticeable. We hypothesized that there is an effect of the lipid types and the iron types on the way the substances concentration effects the R1 values.

The data analysis revealed the relationship between the different types of iron and types of lipids. That is, depending on the type of iron and lipid, there is an effect of the iron and lipid concentrations on the target. In other words, using seaborn library, a scatter plot created to visual the effect of iron types and lipid types on the substances concentration in the goal of predicting R1 values. In Fig. 7 one can clearly detect clusters of common types of lipids and irons.

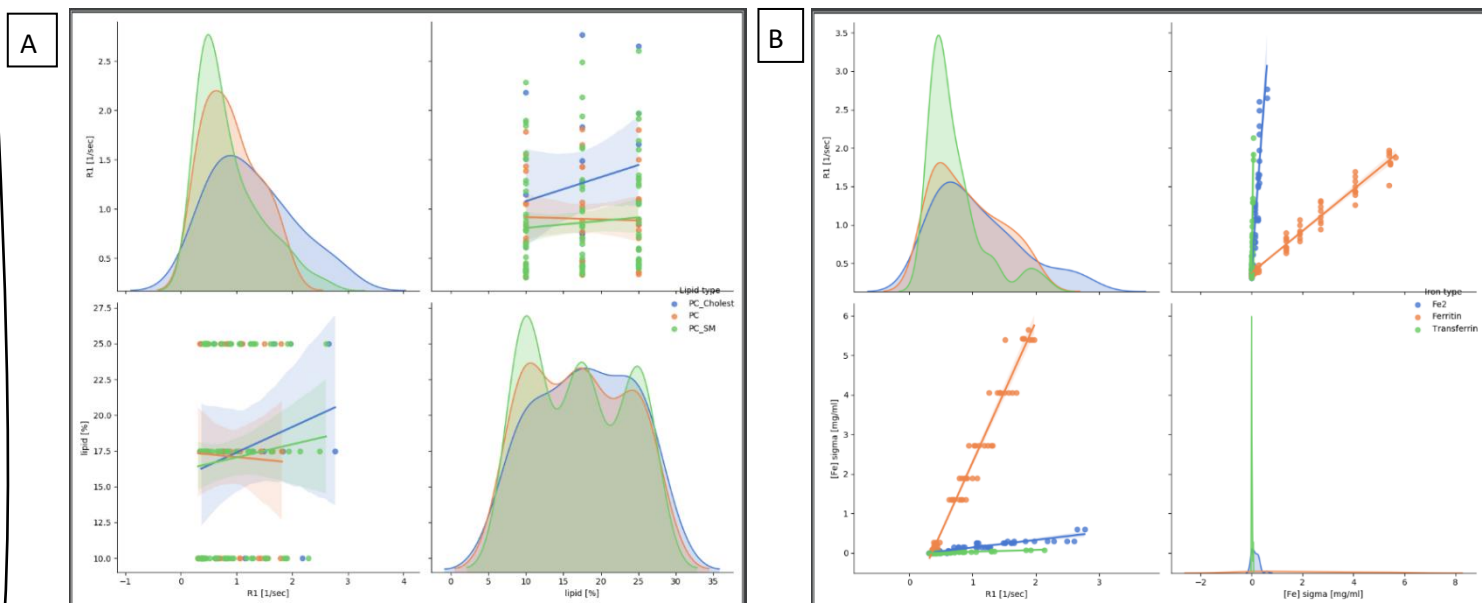


Fig. 7: relations between lipid to R1 and iron to R1 with the effect of lipids and iron types. **A:** pair plot depicting the relationship between lipid concentrations and R1 when common behaviors can be identified for all samples from the same type of lipid. **B:** pair plot depicting the relationship between iron concentrations and R1 when common behaviors can be identified for all samples from the same type of iron.

Due to the last results, linear regression involves interaction between categorical variables (iron types and lipid types) was performed. According to the hypothesis, it was found that when referring to the effect of the types of iron and lipids on the amounts of iron and lipids, respectively, R1 predicted values approximate the real data points very well ($R^2 = 0.926$, $MAE = 0.024$).

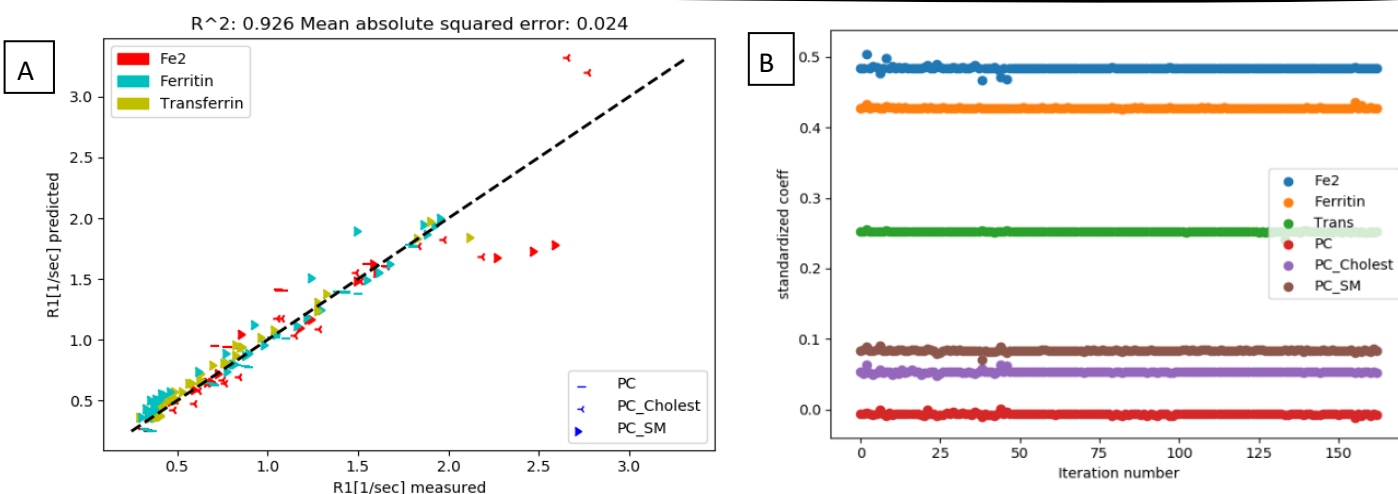


Fig. 8: A: linear regression involves interaction with categorical variables. visualization of the measured R1 values towards the predicted R1 values, which predicted by the equation $R1 = a \cdot [Fe] \cdot \text{iron type} + b \cdot [\text{lipid}] \cdot \text{lipid type} + c$. The presented values transformed cross-validation evaluation, as mentioned in the methods chapter. The R^2 values appearing in the title, and the MAE values, measured in 1/sec units. **B:** As mentioned, each type of iron and each type of lipid paired with another coefficient. The data was standardized using Z-score technique to be able to compare the different coefficients. The graph represents the coefficient of each type during each one of the cross-validation iterations. It can be identified that Fe2 has the most effect on the target, due to its highest coefficient value.

Discussion

In this research, the goal was to find the best fit model that allows to predict R1 values based on lipid and iron concentrations and types. One positive outcome that can be derived from this experiment, is the possibility of inferring diseases and defects in the human brain, depending on the results of R1. Further studies can deduct from this study the relationship between R1 and iron and lipid concentrations, as well as iron and lipid types. Given that relationship, detecting abnormal values of iron and lipid concentrations, can help in diagnostics neurological symptoms and diseases.

In addition to the findings in the literature (Rooney et al., 2007), in this experiment it was found that the types of iron and lipids also influence R1 values prediction, and not just concentrations. As seen in Fig. 8 B, the iron types have more effect than the lipid type, due to its higher coefficient (Cornell & Berger, 1987).

There are some limitations to this research. First, it can be thought that the data is biased. Out of 10 experiments that have been used in this research, not all the combinations of the lipid types and iron types has been tested. The combinations of Ferritin with PC_Cholest, and Transferrin with PC, and PC_Cholest were not included in the phantom system. Due to that fact, it possible that the results supporting the larger meaning of the iron type, won't be demonstrated in future similar experiments. Second, the concentrations presented in this research, are not correlate exactly to the human brain iron and lipid concentrations. Due to that fact, it would not be accurate to draw conclusions about the human brain based on the results of this study (Yeatman et al., 2014).

Further research can aim to model the relation between iron and lipid to other qMRI parameters. With the full models connecting iron and lipids to qMRI parameters, it will be possible to turn the model and find the right equation for predicting iron and lipid in the human brain. These results can lead to innovation in the world of science and medicine.

The code of the research can be found in the following address:

https://github.com/ShirlyEliezer/iron_lipids. In order to download the code to your computer, clone to the desire folder with the command: `git clone https://github.com/ShirlyEliezer/iron_lipids`

References

1. Callaghan, M. F. et al. Widespread age-related differences in the human brain microstructure revealed by quantitative magnetic resonance imaging. *Neurobiol. Aging* 35, 1862–1872 (2014).
2. "Correlation Coefficient: Simple Definition, Formula, Easy Steps". *Statistics How To*, 2021.
3. Yeatman, J. D., Wandell, B. A. & Mezer, A. A. Lifespan maturation and degeneration of human brain white matter. *Nat. Commun.* 5, 4932 (2014).
4. Pearson, Karl (20 June 1895). "Notes on regression and inheritance in the case of two parents". *Proceedings of the Royal Society of London*. 58: 240–242
5. Cox, S. R. et al. Ageing and brain white matter structure in 3,513 UK Biobank participants. *Nat. Commun.* 7, 13629 (2016).
6. David A. Freedman (2009). *Statistical Models: Theory and Practice*. Cambridge University Press. p. 26. *A simple regression equation has on the right hand side an intercept and an explanatory variable with a slope coefficient. A multiple regression equation has on the right hand side, each with its own slope coefficient*
7. Lorio, S. et al. Disentangling in vivo the effects of iron content and atrophy on the ageing human brain. *Neuroimage* 103, 280–289 (2014).
8. Renaud, O., & Victoria-Feser, M. P. (2010). A robust coefficient of determination for regression. *Journal of Statistical Planning and Inference*, 140(7), 1852-1862.
9. Gracien, R.-M. et al. Evaluation of brain ageing: a quantitative longitudinal MRI study over 7 years. *Eur. Radiol.* 27, 1568–1576 (2017).
10. Willmott, Cort J.; Matsuura, Kenji (December 19, 2005). "Advantages of the mean absolute error (MAE) over the root mean square error (RMSE) in assessing average model performance". *Climate Research*. 30: 79–82. doi:10.3354/cr030079.
11. Draganski, B. et al. Regional specificity of MRI contrast parameter changes in normal ageing revealed by voxel-based quantification (VBQ). *Neuroimage* 55, 1423–1434 (2011).
12. T. Hastie, R. Tibshirani, J. Friedman, *The Elements of Statistical Learning*, 2nd edition, Springer, New York/Berlin/Heidelberg, 2008.
13. Tardif, C. L. et al. Investigation of the confounding effects of vasculature and metabolism on computational anatomy studies. *Neuroimage* 149, 233–243(2017).
14. R. Duda, P. Hart, D. Stork, *Pattern Classification*, John Wiley & Sons, 2001.
15. Carey, D. et al. Quantitative MRI provides markers of intra-, inter-regional, and age-related differences in young adult cortical microstructure. *Neuroimage* 182, 429–440 (2017).
16. D. Berrar, W. Dubitzky, Overfitting, in: W. Dubitzky, O. Wolkenhauer, K.-H. Cho, H. Yokota (Eds.), *Encyclopedia of Systems Biology*, Springer, 2013, pp. 1617–1619.
17. Bot, J., Blezer, E., Kamphorst, W., Nijeholt, G., Ader, H.J., Castelijns, J.A., Nicolay, K., Bergers, E., Ravid, R., Polman, C., Barkhof, F., 2004. The spinal cord in multiple sclerosis: relationship of high-spatial-resolution quantitative MR imaging findings to histopathologic results. *Radiology* 233 (2), 531–540
18. Mukaka, M. M. (2012). A guide to appropriate use of correlation coefficient in medical research. *Malawi medical journal*, 24(3), 69-71.
19. Misra, S., Osogba, O., & Powers, M. (2019). Unsupervised outlier detection techniques for well logs and geophysical data. *Machine Learning for Subsurface Characterization*, 1.
20. Benesty, J., Chen, J., Huang, Y., & Cohen, I. (2009). Pearson correlation coefficient. In *Noise reduction in speech processing* (pp. 1-4). Springer, Berlin, Heidelberg.
21. Tabachnick, B. G., Fidell, L. S. (2013) *Using multivariate statistics*, 6th ed. Boston, MA: Pearson.
22. Hamilton, D. F., Ghert, M., & Simpson, A. H. R. W. (2015). Interpreting regression models in clinical outcome studies.
23. Field, A. P., Miles, J. (2010) *Discovering statistics using SAS: (and sex and drugs and rock n roll)*, Thousand Oaks, CA: SAGE.
24. Cornell, J. A., & Berger, R. D. (1987). Factors that influence the value of the coefficient of determination in simple linear and nonlinear regression models. *Phytopathology*, 77(1), 63-70.
25. Tukey, J. W. (1977) *Exploratory data analysis*, Reading, MA: Addison-Wesley.
26. Yeatman, J. D. et al. Lifespan maturation and degeneration of human brain white matter. *Nat. Commun.* 5:4932 doi: 10.1038/ncomms5932 (2014).
27. Shtangel O, Mezer AA. A phantom system for assessing the effects of membrane lipids on water proton relaxation. *NMR in Biomedicine*. 2020; 33: e4209. <https://doi.org/10.1002/nbm.4209>
28. Mottershead, J.P., Schmierer, K., Clemence, M., Thornton, J.S., Scaravilli, F., Barker, G.J., Tofts, P.S., Newcombe, J., Cuzner, M.L., Ordidge, R.J., McDonald, W.I., Miller, D.H., 2003. High field MRI correlates of myelin content and axonal density in multiple sclerosis — a post-mortem study of the spinal cord. *J. Neurol.* 250 (11), 1293–1301
29. Schmierer, K., Scaravilli, F., Altmann, D.R., Barker, G.J., Miller, D.H., 2004. Magnetization transfer ratio and myelin in postmortem multiple sclerosis brain. *Ann. Neurol.* 56(3), 407–415.